RSC Advances

PAPER

View Article Online
View Journal | View Issue

Cite this: *RSC Adv.*, 2026, **16**, 6856

Unraveling the particle size characteristics-flame retardancy relationship in ATH/polyolefin composites: a focus on interfacial properties and thermal decomposition

Huifen Wang, *[ab] Xiongjun Liu,[a] Xiao Han[a] and Lijuan Yuan[a]

This study systematically investigates the influence of ATH particle size characteristics (D_{50} and SPAN) on the flame-retardant performance of ATH/polyolefin composites, and focuses on discussing the potential roles of interface properties and thermal decomposition behavior. Comprehensive analysis reveals that an ATH median particle size (D_{50}) of 2.28 μm, coupled with a SPAN value of 2.19, achieves an optimal balance, facilitating uniform dispersion and strong interfacial adhesion within the polyolefin matrix. This optimal interface not only promotes the formation of a protective char barrier during combustion, as evidenced by a distinct bimodal HRR profile and significantly reduced peak HRR and total heat release values of 129.86 kW m^{-2} and 56.57 MJ m^{-2}, respectively, but also enables the composite material to have the highest tensile strength and elongation at break, demonstrating the synergistic enhancement of flame retardancy and mechanical toughness. TG analysis confirms the superior thermal stability and enhanced residue integrity of this composite. In contrast, deviations from this optimal particle size—toward either finer or coarser distributions—result in particle agglomeration or interfacial defects, respectively, which compromise both flame-retardant efficiency and mechanical properties. Supported by SEM and EDS characterization, this work establishes a clear particle size–interface–performance relationship, providing scientific guideline for the precise design of high-performance flame-retardant polyolefins.

Received 24th November 2025
Accepted 23rd January 2026

DOI: 10.1039/d5ra09056c

rsc.li/rsc-advances

1 Introduction

Low Smoke Zero Halogen (LSOH) flame-retardant materials have gained widespread recognition due to their halogen-free composition, low smoke emission upon heating, and minimal toxicity of combustion products.[1–3] Aluminum trihydroxide (ATH) is one of the most important inorganic flame retardants used in LSOH systems, valued for its non-toxicity, non-corrosiveness, abundance, and low cost.[4,5] The flame-retardant mechanism of ATH is complex, involving the synergy of multiple processes. When heated above 220 °C, ATH undergoes endothermic decomposition, producing non-combustible gases and aluminum oxide.[6] First, the endothermic effect of ATH helps lower the temperature. The released water vapor dilutes flammable gases to delay flame spread, while the resulting active aluminum oxide forms a protective layer on the burning material, which acts as a dense barrier against heat conduction and radiation.[7,8] Additionally, ATH can catalyze the charring of polymer matrices, suppressing the generation of combustible volatiles.[9] Thanks to these multi-phase actions, ATH flame retardants are considered environmentally friendly and exhibit a well-balanced combination of flame retardancy and smoke suppression.

However, optimizing the flame retardant efficiency of ATH during practical incorporation remains a subject worthy of in-depth investigation. For instance, variations in ATH particle size lead to differences in its dispersion within the resin matrix, interfacial compatibility, and reaction kinetics, which are critical factors influencing the combustion performance and mechanical properties of composite polyolefins.[10,11] Furthermore, controlling the particle size of ATH significantly impacts both the production process and application stability. Large ATH particles tend to settle unevenly in polymer materials, resulting in poor dispersion, while fine particles are prone to agglomeration, making processing difficult and compromising compatibility with the matrix.[10,12]

Research on foam silicone rubber by Su *et al.* showed that smaller ATH particles improve mechanical properties like tensile strength but reduce flame retardancy. This non-linear pattern highlights the need to identify an optimal particle size that balances these competing characteristics.[13] Shan *et al.* employed computational modeling to study the flame retardancy of epoxy resin, revealing from a mechanistic perspective

[a]*Academy of Science and Technology, Jiangsu Shangshang Cable Group Co., Ltd., Liyang 213300, China. E-mail: wanghuifen0860@163.com*

[b]*School of Chemical Engineering and Technology, China University of Mining and Technology, Xuzhou 221000, China*

that the incorporation of ATH optimizes the material's peak heat release rate, total heat release, and smoke production rate.[14]

The recent review systematically summarizes the crucial role of microstructure control and interfacial engineering of inorganic fillers (including ATH) in determining the final properties of polymer composites.[15] These analyses emphasize that the characteristics of the fillers, such as particle size, distribution, and morphology, are fundamental variables that determine dispersion, interface stress transfer, and thermal–mechanical properties.[16,17] This established knowledge system confirms that manipulating the particle structure of ATH is a powerful means for material design.

Although significant progress has been made and the general principles of filler microstructure–property relationships are well-recognized,[15,16] a unified and systematic understanding of how ATH particle size characteristics (both median diameter and distribution width) synergistically govern the interfacial properties, thermal decomposition, and fire behavior in highly-filled polyolefin systems specifically designed for LSOH cable sheathing remains conspicuously lacking.[10,18–23] In particular, in industrial applications where high load conditions (such as 180 phr) are very common, the optimal balance state remains unclear due to the significant increase in processing and interface-related challenges.

To address the aforementioned issues, this paper selects ATH with different particle sizes as the research subject. Utilizing test methods such as oxygen index, smoke density, and cone calorimetry, it systematically analyzes the combustion behavior of these flame retardants within an LSOH system. Combined with microstructural characterization, the flame retardant mechanism is elucidated, providing a robust theoretical foundation and technical solution for optimizing ATH particle size distribution and developing high-performance, environmentally friendly flame retardant materials.

2 Experimental section

2.1 Main raw materials

Ethylene-vinyl acetate (EVA): Yangzi Petrochemical-BASF, 6110MC; metallocene-catalyzed linear low-density polyethylene (mLLDPE): ExxonMobil, 3518CB; ethylene–octene copolymer (POE): Mitsui Chemicals, Japan, DF810; maleic anhydride grafted polyethylene (MAH-PE): Supo, BP-10M; polyethylene wax: Cesar Success, 2420; silicone: Wujiang, PMAF-15; antioxidant 1: Tiansheng Chemical, Tianjin, 1010; antioxidant 2: Tiansheng Chemical, Tianjin, 168; silane coupling agent: Shandong Silike New Material, S230; ATH powders with different particle sizes: 1.35 μm (ATH-1), 1.61 μm (ATH-2), 2.28 μm (ATH-3), 2.80 μm (ATH-4), 4.11 μm (ATH-5), 9.82 μm (ATH-6), 17.77 μm (ATH-7), respectively.

2.2 Major equipment and instruments

Torque rheometer: Harbin Hapro Electric Technology Co., Ltd, model RM-200A.

Precision two-roll mill: Dongguan Zhenggong Electromechanical Equipment Technology Co., Ltd, model ZG-YR-120.

Precision automatic tablet press: Dongguan Zhenggong Electromechanical Equipment Technology Co., Ltd, model ZG-20T.

Flat vulcanizing machine: Huzhou Hongchuan Rubber Machinery Factory, model XLB-D/Q.

Cone calorimeter: FTT (UK), Dual Cone Calorimeter.

Oxygen index analyzer: FTT (UK), Oxygen Index.

NBS smoke density chamber: Mottisco Combustion Technology Instruments (Kunshan) Co., Ltd, model SDB.

UL-94 horizontal and vertical burning test chamber: Shengyuan Systech Co., Ltd, model RH-6033A.

Thermogravimetric analyzer (TGA): Netzsch, model TG 209 F3 Tarsus®.

Scanning electron microscope (SEM): ZEISS (Germany), model Sigma 360.

Universal testing machine: Shanghai Hualong Test Instruments, WDW-0.5C.

Laser particle size analyzer: Dandong Baite Instrument Co., Ltd, BT-9300ST.

2.3 Sample preparation

The base experimental formulation was as follows: EVA 62 phr, PE 20 phr, POE 10 phr, MAH-PE 8 phr, polyethylene wax 2 phr, silicone 5 phr, antioxidant 1010 0.5 phr, antioxidant 168 0.5 phr, silane coupling agent 1%, and ATH 180 phr. The ATH loading of 180 phr was selected to replicate the practical formulations used in industrial LSOH cable sheathing compounds, allowing for the evaluation of performance under real-world application conditions. To investigate the effect of ATH particle size, the polyolefin matrix and other additives were kept constant, with ATH particle size as the sole variable.

Weighed raw materials according to the formulation were melt-blended using a torque rheometer at 140 °C for 15 minutes. The mixture was then sheeted on a two-roll mill at 130 °C. Subsequently, polyolefin sheet materials were obtained through hot pressing (180 °C, 10 min) followed by cold pressing using the flat vulcanizing machine. These sheets were finally cut into test specimens.

Based on the different ATH particle sizes used, the prepared samples were designated as LSOH-1 (ATH median particle size D_{50} = 1.35 μm), LSOH-2 (D_{50} = 1.61 μm), LSOH-3 (D_{50} = 2.28 μm), LSOH-4 (D_{50} = 2.80 μm), LSOH-5 (D_{50} = 4.11 μm), LSOH-6 (D_{50} = 9.82 μm), and LSOH-7 (D_{50} = 17.77 μm).

2.4 Performance testing standards

Combustion test. The flame retardancy of the composite polyolefin materials was evaluated using a cone calorimeter (FTT, UK) according to the standard GB/T 16172-2007 "Test Method for Heat Release Rate of Building Materials".

Limiting oxygen index (LOI) test. The room temperature LOI was determined according to GB/T 2406.2-2009 "Plastics – Determination of burning behavior by oxygen index – Part 2: Ambient-temperature test". The high-temperature LOI was determined according to GB/T 2406.3-2022 "Plastics –

Determination of burning behavior by oxygen index – Part 3: Elevated-temperature test".

Smoke density test. Smoke density under smoldering and flaming conditions was tested according to ISO 5659-2:2017 "Plastics-Smoke generation-Part 2: Determination of optical density by a single-chamber test".

Vertical burning test. The flame retardant rating (UL-94) was assessed according to GB/T 2408-1996 "Plastics-Test Method for Flammability by Horizontal and Vertical Methods".

Mechanical property test. The tensile strength and elongation at break were tested on a universal testing machine in accordance with GB/T 1040.3-2006 "Determination of tensile properties of plastics-Part 3: Test conditions for films and sheets" at a tensile speed of 100 mm min^{-1}.

3 Results and discussion

3.1 Effect of ATH particle size on the combustion performance of the LSOH flame-retardant system

As shown in Table 1, all samples (thickness: 3 mm) achieved a V-0 rating when exposed to an open flame, with no dripping observed during the process. This indicates that the addition of ATH effectively ensures good flame retardancy and self-extinguishing properties of the material. Furthermore, the Limiting Oxygen Index (LOI) of the composite polyolefins exhibited a non-monotonic relationship with ATH particle size. As the ATH particle size increased from 1.35 μm to 2.28 μm, the ambient-temperature LOI rose to 37.3%. However, with further increase in particle size, the ambient-temperature LOI decreased significantly. Similarly, for samples LSOH-1 to LSOH-5, the high-temperature LOI ranged between 32.0% and 34.8%, with LSOH-3 exhibiting the highest value (34.8%). Subsequently, from LSOH-5 to LSOH-7, the high-temperature LOI decreased to 29.6% and 28.3%, respectively. This consistent trend between high-temperature and ambient-temperature LOI, peaking for LSOH-3, further validates the influence of particle size on flame retardant performance.

The aforementioned phenomenon can be attributed to a particle size threshold effect. When the ATH particle size is small, the larger specific surface area promotes good dispersion within the matrix, effectively enhancing flame retardant efficiency. However, when the particle size exceeds a certain threshold, it negatively impacts the oxygen index, likely due to issues such as filler agglomeration and poor dispersion caused by excessively large particles, which adversely affect the material's thermal stability and char-forming ability.[19,24] Therefore, during the material design phase, determining the "optimal particle size range" is crucial for ensuring optimized flame retardant performance.

Smoke density testing can objectively quantify the amount of smoke generated by LSOH materials upon exposure to fire, serving as a key indicator for assessing the safety grade of polyolefins.[25] Fig. 1 presents the smoke density test results of composite polyolefins with different ATH particle sizes, obtained under the ISO 5659 standard. Under flaming conditions, LSOH-3 exhibited the lowest maximum specific optical density of merely 42.44, demonstrating superior low-smoke characteristics. Under non-flaming conditions, LSOH-1 with the smallest particle size showed the highest smoke density (360.85). As the particle size gradually increased (LSOH-2, LSOH-3, and LSOH-4), the smoke density decreased significantly to approximately 280. However, with further increases in particle size (LSOH-5, LSOH-6, and LSOH-7), the smoke suppression capability of the materials progressively deteriorated.

ATH with smaller particle size has a larger specific surface area and higher surface energy, which leads to particle agglomeration.[26,27] Therefore, uneven and incomplete combustion reactions bring about an increase in the production of smoke. Furthermore, the expanded ATH surface area facilitates more efficient contact with heat and flammable gases, accelerating the decomposition process and generating a large amount of water vapor. The micro "explosion effects" on the surface of polyolefin materials have destroyed the dense protective char layer barrier. The activated alumina obtained by ATH decomposition possesses high surface acidity and catalytic activity, which can catalyze specific pyrolysis reactions, thus generating more small molecule unsaturated hydrocarbons and aromatic compounds, and promoting smoke formation in polymers.[28]

Table 1 Vertical burning test results and oxygen index of composite polyolefins with different ATH particle sizes

Samples	UL-94 rating (3 mm)	Dripping	LOI/%	
			Ambient-temp. LOI	High-temp. LOI
LSOH-1	V-0	No	35.2	32.0
LSOH-2	V-0	No	35.7	33.2
LSOH-3	V-0	No	37.3	34.8
LSOH-4	V-0	No	36.1	34.1
LSOH-5	V-0	No	35.3	33.0
LSOH-6	V-0	No	31.6	29.6
LSOH-7	V-0	No	30.4	28.3

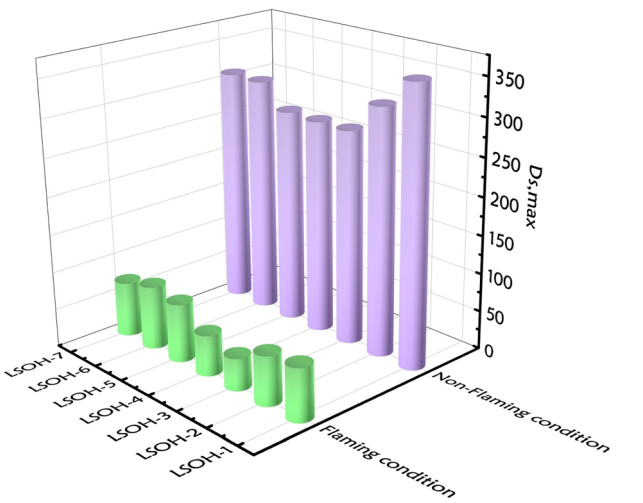

Fig. 1 Smoke density test results of composite polyolefins with different ATH particle sizes under flaming and non-flaming conditions.

Table 2 Cone calorimeter test results of composite polyolefins with different ATH particle sizes

Samples	TTI (s)	pHRR (kW m^{-2})	THR (MJ m^{-2})
LSOH-1	68	186.47	63.42
LSOH-2	72	157.27	59.26
LSOH-3	62	129.86	56.57
LSOH-4	62	144.41	54.67
LSOH-5	60	174.20	63.68
LSOH-6	59	189.67	67.89
LSOH-7	55	212.47	70.40

Conversely, large-particle ATH have poor dispersion and cause defects within the matrix, serving as pathways for smoke and flame penetration, also resulting in substantial smoke production.[29]

To systematically investigate the impact of aluminum hydroxide (ATH) particle size on the practical fire safety of polyolefin composites, this study evaluated the combustion performance of the materials using a cone calorimeter at the heat flux of 50 kW m^{-2}. By analyzing key parameters such as time to ignition (TTI), peak heat release rate (pHRR), and total heat release (THR) (as presented in Table 2), it was found that the particle size of ATH significantly influences the flame retardancy of the materials.

Fig. 2a shows the heat release rate (HRR) curves of these seven materials. LSOH-3 exhibits a typical bimodal peak structure ("rise-suppression-release" pattern). After ignition, the first heat release peak appears. During this stage, ATH decomposes in an endothermic manner and gradually forms a protective char layer, which inhibits flame spread and causes the HRR to decrease. When the heat accumulates to a certain extent, causing the carbon layer to break or undergo deep decomposition, a second lower-intensity and wider heat release peak will form. The entire HRR curve of LSOH-3 is well-defined and smooth, indicating an orderly and controlled combustion process. In contrast, the HRR curves of other samples show multiple irregular peaks or a jagged, fluctuating pattern, suggesting an unstable combustion process and a lower flame retardant efficiency.

Specifically, when the ATH particle size was 2.28 μm, LSOH-3 exhibited the lowest pHRR (129.86 kW m^{-2}). This represents reductions of approximately 30% and 39% compared to the smallest particle size sample, LSOH-1 (186.47 kW m^{-2}), and the largest particle size sample, LSOH-7 (212.47 kW m^{-2}), respectively. Its performance was also significantly superior to other samples. Furthermore, the THR of LSOH-3 was only 56.57 MJ m^{-2}, indicating a lower total heat release during combustion and suggesting a reduced fire load.

Importantly, to accurately assess the material's "hazard" in a real fire scenario, we specifically calculated the Fire Performance Index (FPI = TTI/pHRR). Generally, the FPI value correlates positively with fire safety; a higher FPI indicates a longer duration from ignition to intense burning, implying higher fire safety.[30] As shown in Fig. 2b, the particle size increases progressively from LSOH-1 to LSOH-7. However, the FPI value does not change monotonically with particle size; instead, there is an optimal balance point between combustion performance and particle size (LSOH-3).

In summary, due to the moderate particle size of ATH in LSOH-3, this material achieved the best flame retardant efficiency, attaining an optimal balance between good dispersion and stable decomposition.

3.2 Analysis of thermal stability of composite polyolefins with different ATH particle sizes

Fig. 3 presents the TG and corresponding DTG curves of the composite polyolefins filled with ATH of different particle sizes. All samples primarily underwent two or three distinct thermal degradation stages.

Table 3 details the three main mass loss stages and the final residue yield for the seven polyolefin samples containing ATH of different particle sizes during the thermogravimetric test. Preliminary analysis indicates that the flame retardant particle size systematically influences the thermal decomposition behavior of the polyolefins.

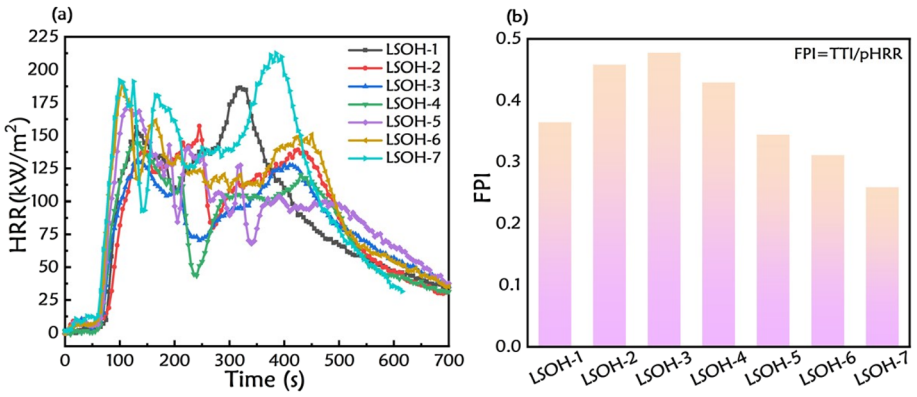

Fig. 2 (a) Heat release rate (HRR) curve and (b) fire performance index (FPI) bar chart of ATH composite polyolefin with different particle sizes at the heat flux of 50 kW m^{-2}.

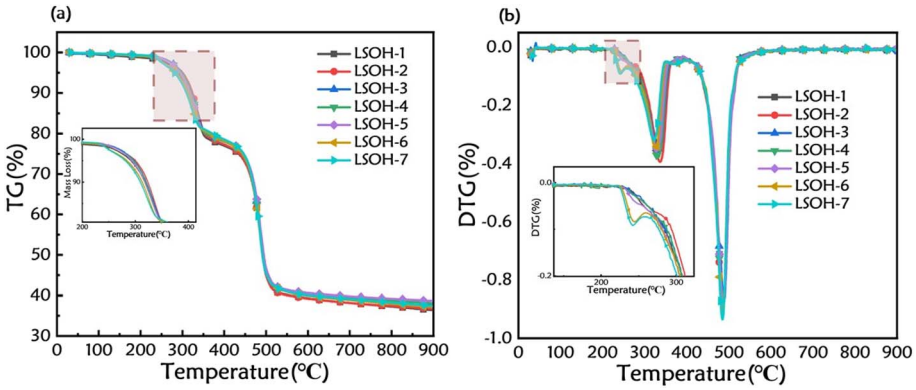

Fig. 3 (a) TG and (b) DTG curves of polyolefin composites with ATH of different particle sizes.

Table 3 Derivative thermogravimetry (DTG) analysis of composite polyolefins with different ATH particle sizes

Samples	T_{p1} (°C)	R_1 (%/min)	T_{p2} (°C)	R_2 (%/min)	T_{p3} (°C)	R_3 (%/min)	Residue yield (%)
LSOH-1	—	—	337.21	−7.34	489.88	−17.03	36.44
LSOH-2	—	—	337.77	−7.92	487.73	−20.88	36.76
LSOH-3	—	—	334.10	−7.83	492.70	−19.41	37.97
LSOH-4	—	—	330.79	−7.53	487.73	−17.13	38.10
LSOH-5	—	—	329.40	−6.97	484.48	−19.56	38.71
LSOH-6	244.46	−1.77	326.80	−6.97	483.14	−20.85	37.18
LSOH-7	242.07	−1.89	322.03	−6.35	486.55	−21.32	37.48

Firstly, the first mass loss peak (T_{p1}) was observed only in LSOH-6 and LSOH-7. This is a negative sign, suggesting that the large ATH particles possess unstable structures, causing premature decomposition of these materials around 240 °C. This prevents their decomposition from cooperating with the decomposition of the polymer matrix, resulting in a decrease in the flame retardant efficiency. This discover correlates well with the higher pHRR and THR values observed for LSOH-6 and LSOH-7 in the cone calorimeter tests. Furthermore, LSOH-7 exhibited the highest mass loss rate in the third stage (absolute value of R_3), which also indicates that the large particle components decomposed more intensely at high temperatures, which is not conducive to the impact resistance performance of the material in real fire scenarios. Around 330 °C, the materials produced a second mass loss peak (T_{p2}), resulting mainly from the overlapping decomposition of the polyolefin matrix and the majority of the ATH. As the particle size increased (from LSOH-2 to LSOH-7), T_{p2} showed a linear decreasing trend. This is because smaller particle sizes provide ATH powder with a larger specific surface area, leading to more uniform heat transfer upon heating and thus relatively better thermal stability. The third mass loss peak (T_{p3}) occurred mainly between 480–490 °C, primarily corresponding to the continued decomposition of ATH, further oxidative decomposition of the char formed from the polymer, or the volatilization of the deep decomposition products of the polymer. LSOH-3 exhibited the highest peak temperature (492.70 °C) for this stage, indicating superior high-temperature stability in the later stages. The residue (char/Al_2O_3 composite layer) formed by LSOH-3 is the most stable at high temperatures and the most resistant to further oxidative decomposition. The residue yield refers to the proportion of inert substances like aluminum oxide formed after high-temperature decomposition and is often related to the quality of the flame-retardant char.[31] LSOH-3 had a residue yield of 37.97%. This favorable residue yield indicates good char-forming ability for this material.

In summary, LSOH-3 demonstrated the best overall performance, exhibiting balanced and stable behavior across the entire temperature range, while simultaneously achieving good high-temperature stability and residue yield.

3.3 Laser particle size analysis of ATH powders

Fig. 4a–g presents the laser particle size measurement results for the different ATH powders. The cumulative particle size distribution curves indicate that the median particle sizes (D_{50}) of the ATH powders are 1.35, 1.61, 2.28, 2.80, 4.11, 9.82, and 17.77 μm, respectively. The particle size distribution histograms reveal that all ATH samples exhibit a unimodal distribution, yet with notable differences in distribution breadth and sharpness. The SPAN value provides a direct measure of the breadth of the particle size distribution; a smaller SPAN value indicates a narrower distribution and greater particle uniformity, whereas a larger value reflects a broader distribution with increased heterogeneity in particle size.[32] As shown in Fig. 4h, ATH-1 and ATH-2 exhibit the highest degree of particle size uniformity (lowest SPAN values). However, in practice, their excessively small absolute particle sizes may induce issues such as agglomeration, which can limit performance enhancement. In contrast, although ATH-3 does not

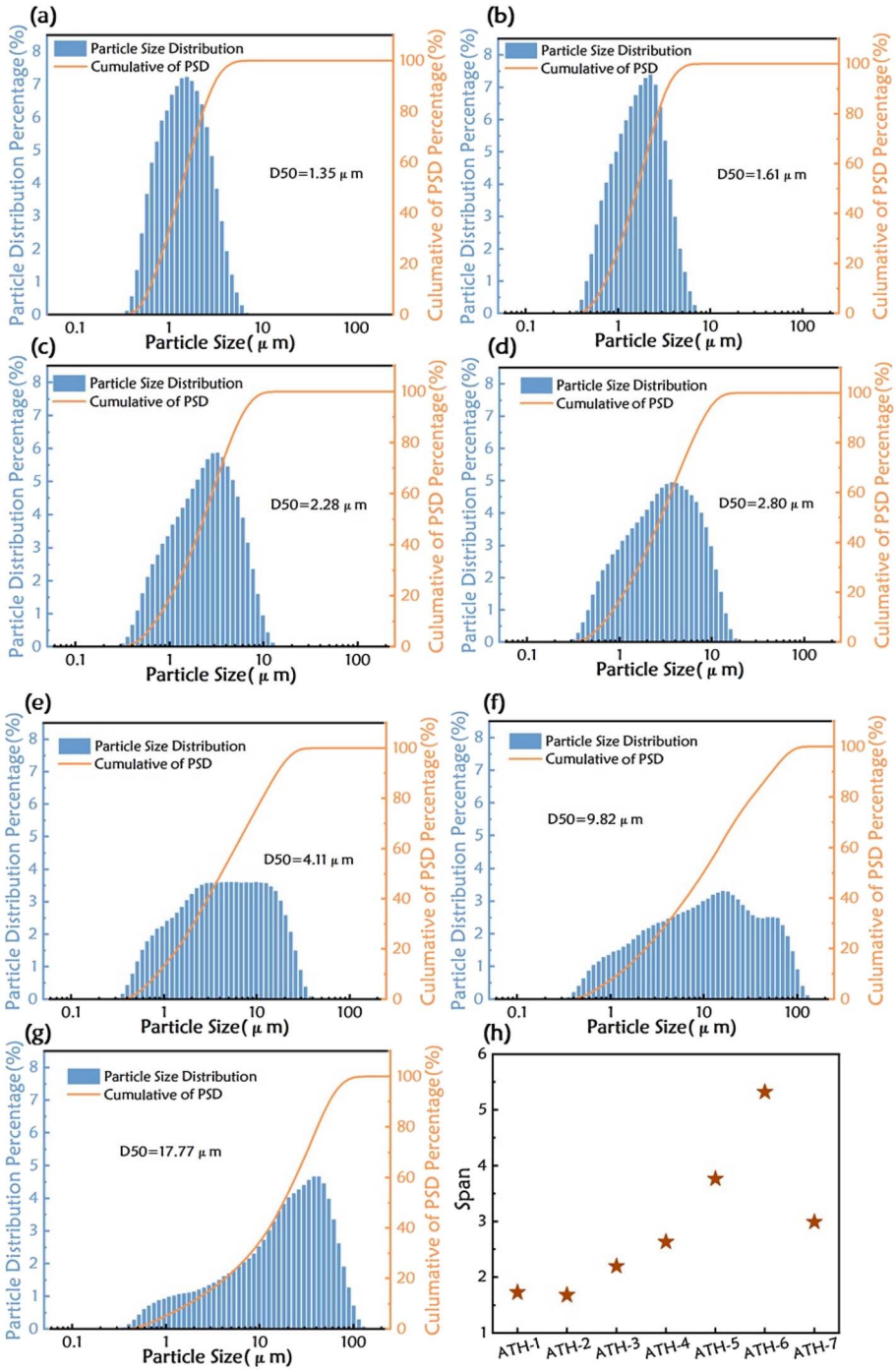

Fig. 4 (a–g) Histograms of particle size distribution and cumulative particle size curves of ATH powders with different particle sizes; (h) SPAN values.

possess the lowest SPAN value (2.19), its moderate distribution width signifies a gradient structure comprising a balanced proportion of fine and coarse particles. According to the particle packing theory, such a polydisperse distribution is conducive to achieving a higher packing density within the polymer matrix, because finer particles can effectively fill the interstices between larger ones. We infer that this denser packed microstructure facilitates the formation of a more continuous and less porous char/Al_2O_3 composite barrier during combustion, thereby enhancing its effectiveness in insulating heat and mass transfer. Consequently, the optimal flame-retardant performance of ATH-3 arises from a synergistic balance between its median particle size (D_{50} = 2.28 μm) and its moderate distribution width (SPAN = 2.19). On the other hand, the SPAN values deteriorate significantly for ATH-4 to ATH-7, reaching an extreme of 5.32 for ATH-6. This indicates a broad and heterogeneous particle population,

resulting in a low packing density, numerous interfacial defects, and inconsistent thermal behavior-which is consistent with the premature decomposition phenomenon observed in the corresponding TG curve.

3.4 Comparison of the optimal ATH size with existing literature

The optimal ATH particle size (D_{50} = 2.28 μm) determined for the highly filled polyolefin composites (180 phr) in this work differs from the reported values for other polymer systems, highlighting the system-dependent nature of filler optimization. For instance, in epoxy resin composites, which the primary goal is mechanical reinforcement with moderate flame retardancy, studies have frequently focused on sub-micron or nano-sized ATH to maximize the interfacial area and stress transfer.[33] Conversely, in EVA copolymers, several reports suggest optimal ATH particle sizes around 1 μm for achieving a good compromise between flame retardancy and mechanical flexibility at common loadings.[34]

Herein, our work addresses a high-loading (180 phr) polyolefin blend for LSOH cable sheathing. Excessively fine particles (*e.g.* sub-micron) can lead to severe agglomeration, increased melt viscosity, and poor dispersion, affecting the processing and the formation of a coherent protective char. Therefore, the identified optimum of 2.28 μm, in conjunction with the moderate distribution width (SPAN = 2.19), represents a scenario-specific finding. It demonstrates that for such demanding systems, a moderate micron-scale particle size combined with an optimized distribution is critical for achieving uniform dispersion, strong interfacial adhesion and effective char formation, rather than simply minimizing particle size. This conclusion highlights the significance of tailoring the characteristics (size and distribution) of filler particles based on the specific constraints and performance requirements of the composite material system.

3.5 Morphological analysis of composite polyolefins with different ATH particle sizes

To deeply investigate the microscopic mechanism underlying the influence of different ATH particle sizes on the flame retardancy of the composite polyolefin, a series of samples were cryogenically fractured in liquid nitrogen, and the cross-sectional morphology (SEM) and aluminum element distribution (EDS) were examined. As shown in Fig. 5a–g, the particle size of ATH determines its dispersion state within the polyolefin matrix. For samples with smaller particle sizes, namely LSOH-1 (Fig. 5a), LSOH-2 (Fig. 5b), and LSOH-3 (Fig. 5c), the fracture surfaces observed by SEM are relatively smooth and uniform. EDS mapping does not show obvious aggregation; instead, Al is highly dispersed and evenly distributed within the matrix, indicating that the ATH particles in the composite material have good dispersion and have formed a uniform phase structure. Although there are slight differences in form among these three materials, LSOH-3 exhibited the most outstanding flame-retardant performance. This can be attributed to the fact that its particle size distribution has reached the "optimal point", enabling ATH to rapidly and effectively absorb heat during the thermal decomposition process, release water vapor, and simultaneously work in synergy with the matrix to form a continuous, and stable protective carbon layer.

As the ATH particle size increases (Fig. 5d–g), the particle structure and roughness on the fracture surface of the material become increasingly evident, especially in LSOH-6 and LSOH-7. EDS reveals that the distribution of the Al element presents

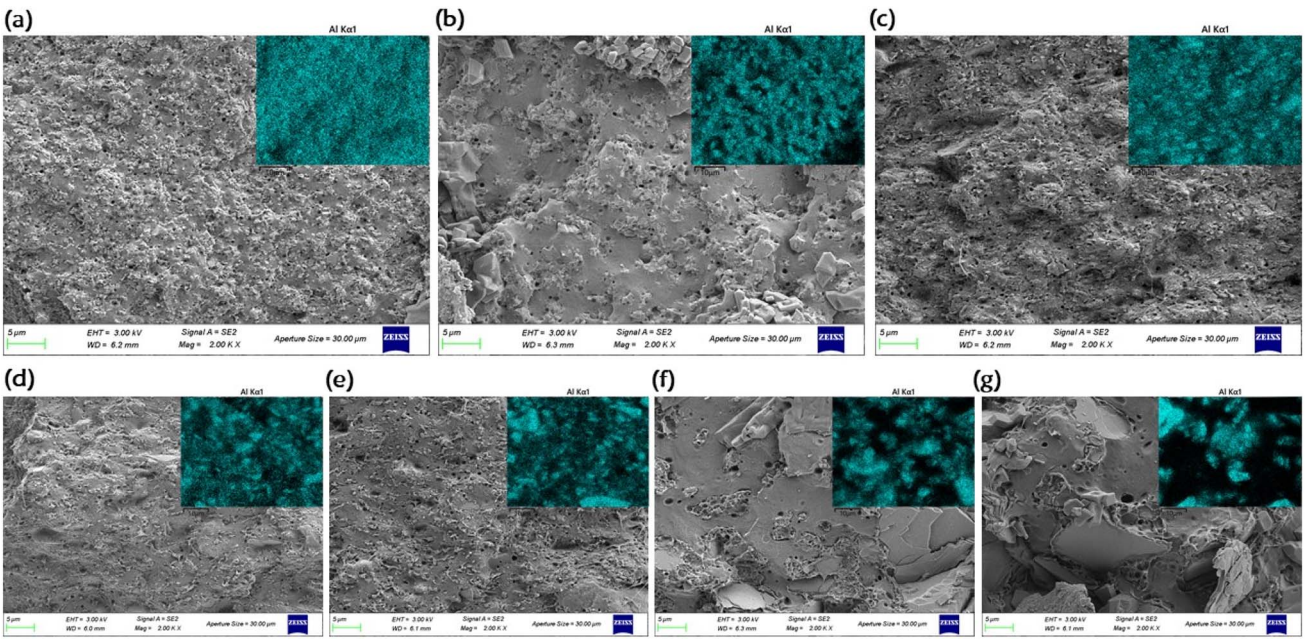

Fig. 5 Cryogenically fractured cross-sectional SEM images (a–g) and corresponding EDS maps of Al distribution (insets) for composite polyolefins with different ATH particle sizes.

concentrated, patch-like bright spots, indicating that the ATH has poor dispersion within the matrix and there is a distinct phase boundary. The interfacial adhesion between the large ATH particles and the matrix is weak, which can act as a defect, hindering the formation of carbon and making the flame and heat more likely to penetrate. Furthermore, the internal thermal decomposition of large ATH particles is insufficient, and the synergistic interaction with the polymer matrix is reduced, leading to incomplete and uneven flame-retardant reactions during combustion.

Overall, considering both the microscopic morphology and macroscopic flame retardancy performance, the particle size and dispersion state of ATH are key factors determining the flame retardancy performance of the composite polyolefin. Therefore, in practical applications, selecting ATH with an appropriate particle size and uniform dispersion is crucial for achieving the best flame retardancy performance during combustion.

3.6 Analysis of mechanical performance

To evaluate the practical mechanical significance of ATH particle size at the high loading of 180 phr, tensile tests were conducted. The results of tensile strength and elongation at break are presented in Fig. 6. As demonstrated, both properties follow a consistent trend: they increase initially with increasing ATH particle size, reach a maximum at a D_{50} of approximately 2.28 μm (LSOH-3), and then decrease with further size increases. This non-monotonic behavior correlates with the dispersion and interfacial characteristics revealed by SEM (Section 3.5). The LSOH-3 exhibits the most uniform distribution of fillers and the fewest interface defects. Therefore, it has the strongest tensile strength and the greatest elongation before fracture (resilience).

This can be attributed to the critical role of the filler–matrix interface. A homogeneous microstructure without large agglomerates or voids prevents premature crack initiation, preserving the material's ductility. Conversely, the agglomeration of fine particles (*e.g.*, in LSOH-1, LSOH-2) and the poor adhesion of coarse particles (*e.g.*, in LSOH-5 to LSOH-7) act as stress concentrators, leading to earlier failure and thus lower strength and elongation. Therefore, the optimized ATH particle size (2.28 μm) not only enhances the flame retardancy but also improves the mechanical integrity of the composite material, highlighting its comprehensive applicability in the practical application of LSOH cable sheaths.

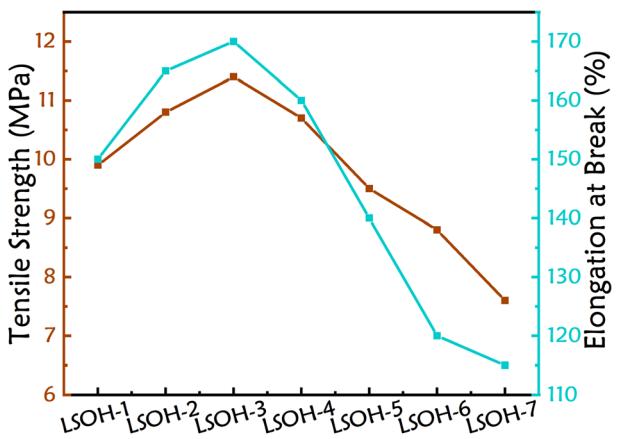

Fig. 6 Tensile properties of composite polyolefins with different ATH particle sizes.

4 Conclusion

In conclusion, this study has clarified the crucial role of the particle size of ATH in determining the flame retardancy and mechanical properties of polyolefin composites by controlling its interface structure and thermal degradation behavior. Experiments demonstrate that ATH with a moderate particle size (*e.g.*, LSOH-3) establishes a synergistic mechanism of "excellent dispersion-strong interfacial adhesion-efficient char formation-enhanced mechanical integrity". During the combustion process, this synergy promotes the formation of a continuous char/Al_2O_3 composite barrier, which effectively inhibits heat and mass transfer, thereby yielding the lowest heat release rates. Simultaneously, the optimal interface directly translates to superior mechanical performance, as evidenced by LSOH-3 achieving the highest tensile strength (11.4 MPa) and greatest elongation at break (170%) among all composites. This confirms that the enhancements in flame retardancy and mechanical toughness are mutually reinforcing outcomes originating from the same microstructural optimum. On the contrary, deviating from this optimal particle size disrupts this synergistic effect: excessively fine particles promote agglomeration, while overly coarse particles lead to weak interfaces and defects. These conditions result in incomplete protective barriers and compromised mechanical properties, as seen in the inferior fire performance and reduced tensile strength/ductility of the other samples.

The "particle size-interfacial structure-multifunctional performance" correlation model established herein provides a fundamental theoretical framework and a practical approach for designing high-performance halogen-free flame-retardant polyolefins. It demonstrates that by precisely controlling the filler's particulate characteristics, one can concurrently tailor both the fire safety and the mechanical reliability of the composite, which is an essential strategy for developing advanced LSOH cable materials.

Author contributions

Huifen Wang: writing-original draft, visualization, validation, investigation, formal analysis, data curation; Xiongjun Liu: supervision, resources, conceptualization, writing-review & editing, methodology; Xiao Han: project administration, validation, methodology, conceptualization; Lijuan Yuan: validation, methodology, conceptualization.

Conflicts of interest

There are no conflicts to declare.

Data availability

The authors confirm that the data supporting the finding of this study are available within the article. Additional information can be provided from the corresponding author upon request.

References

1 A. Porfyris, A. Vafeiadis, C. Gkountela, C. Politidis, G. Messaritakis, E. Orfanoudakis, S. Pavlidou, D. Korres, A. Kyritsis and S. Vouyiouka, *Polymers*, 2024, **16**, 1298.
2 M. Thirumal, D. Khastgir, G. Nando, Y. Naik and N. Singha, *Polym. Degrad. Stab.*, 2010, **95**, 1138–1145.
3 B. Liu, H. Zhao and Y. Wang, *Adv. Mater.*, 2022, **34**, 2107905.
4 F. Laoutid, L. Bonnaud, M. Alexandre, J. Lopez-Cuesta and P. Dubois, *Mater. Sci. Eng., R*, 2009, **63**, 100–125.
5 L. Du and B. Qu, *J. Mater. Chem.*, 2006, **16**, 1549–1554.
6 L. Yu, L. Chen, L. Dong, L. Li and Y. Wang, *RSC Adv.*, 2014, **4**, 17812–17821.
7 S. Elbasuney, *Powder Technol.*, 2017, **305**, 538–545.
8 J. Vaari and A. Paajanen, *Comput. Mater. Sci.*, 2018, **153**, 103–112.
9 Y. Liu, Z. Tang and J. Zhu, *J. Appl. Polym. Sci.*, 2022, **139**, DOI: 10.1002/app.53168.
10 A. Perthué, P. Bussière, M. Baba, J. Larche, S. Therias, F. Karasu and C. Croutxé-Barghorn, *Prog. Org. Coat.*, 2018, **114**, 145–153.
11 I. Joni, T. Nishiwaki, K. Okuyama, S. Isoi and R. Kuribayashi, *Powder Technol.*, 2010, **204**, 145–153.
12 K. Geng, J. Yao, J. Lu, P. Sun, L. Cui and Y. Dong, *Fuel*, 2022, **328**, 125342.
13 J. Su, M. Li, X. Zeng, X. Wu and B. Luo, *Silicone Mater.*, 2019, **33**, 467–470.
14 X. Shan, M. Zhang, J. Zhang, L. Li, Y. Song and J. Li, *Chem. Ind. Eng. Prog.*, 2023, **42**, 3413–3419.
15 M. Meucci, S. Haveriku, M. Badalassi, C. Cardelli, G. Ruggeri and A. Pucci, *Micro*, 2022, **2**, 164–182.
16 S. Haveriku, M. Meucci, M. Badalassi, C. Cardelli and A. Pucci, *Micro*, 2022, **2**, 524–540.
17 X. Liu, Q. Shen, C. He, Y. Yang, X. Han and Q. Xie, *J. Therm. Anal. Calorim.*, 2025, **150**, 11799–11807.
18 M. Sabet, A. Hassan and C. Ratnam, *Int. Polym. Process.*, 2013, **28**, 393–397.
19 M. Yang and B. Yuan, *Materials*, 2025, **18**, 984.
20 M. Chang, S. Hwang and S. Liu, *J. Ind. Eng. Chem.*, 2014, **20**, 1596–1601.
21 C. Lee, S. Kim, J. Nam and K. Suh, *Polym. Eng. Sci.*, 2000, **40**, 857–862.
22 F. Tomiak, B. Schartel, M. Wolf and D. Drummer, *Polymers*, 2020, **12**, 1315.
23 M. Parida, S. Mohanty, M. Biswal, S. Nayak and S. Rai, *J. Therm. Anal. Calorim.*, 2023, **148**, 807–819.
24 L. Wu and Q. Luo, *Spec. Purp. Rubber Prod.*, 2011, **32**, 18–22.
25 Y. Huang and C. Wu, *Opt. Fiber Electr. Cable Appl.*, 2022, **4**, 18–20.
26 A. Tsuda and N. Konduru, *Nanoimpact*, 2016, **2**, 38–44.
27 C. Bantz, O. Koshkina, T. Lang, H. Galla, C. Kirkpatrick, R. Stauber and M. Maskos, *Beilstein J. Nanotechnol.*, 2014, **5**, 1774–1786.
28 D. Lundie, A. McInroy, R. Marshall, J. Winfield, P. Jones, C. Dudman, S. Parker, C. Mitchell and D. Lennon, *J. Phys. Chem. B*, 2005, **109**, 11592–11601.
29 E. Gunel and C. Basaran, *Mech. Mater.*, 2013, **57**, 134–146.
30 W. Luo, M. Chen, T. Wang, J. Feng, Z. Fu, J. Deng, Y. Yan, Y. Wang and H. Zhao, *Nat. Commun.*, 2024, **15**, 2726.
31 B. Szolnoki, K. Bocz, G. Marosi and A. Toldy, *Polymers*, 2016, **8**, 322.
32 Y. de Lafuente, E. Quarta, M. Magi, A. Apas, J. Pagani, M. Palena, P. Páez, F. Sonvico and A. Jimenez-Kairuz, *Antibiotics*, 2025, **14**, 169.
33 D. Gkiliopoulos, D. Bikiaris, D. Efstathiadis and K. Triantafyllidis, *J. Compos. Sci.*, 2023, **7**, 243.
34 L. Zhang, C. Li, Q. Zhou and W. Shao, *J. Mater. Sci.*, 2007, **42**, 4227–4232.